Critical behavior of the ferromagnetic perovskites RTiO_{3} (R = Dy, Ho, Er, Tm, Yb) by magnetocaloric measurements

Yantao Su, Yu Sui, J.-G. Cheng, J.-S. Zhou, Xianjie Wang, Yang Wang, and J. B. Goodenough

Phys. Rev. B **87**, 195102 — Published 2 May 2013

DOI: 10.1103/PhysRevB.87.195102

Critical behavior of the ferromagnetic perovskites $RTiO_3$ (R = Dy, Ho, Er, Tm, Yb) by magnetocaloric measurements

Yantao Su[1], Yu Sui[1,*], J.-G Cheng[2,3], J.-S Zhou[2], Xianjie Wang[1], Yang Wang[1] and J.B. Goodenough[2]

[1]Department of Physics, Harbin Institute of Technology, Harbin 150001, China

[2]Texas Materials Institute, University of Texas at Austin, Austin, Texas 78712, USA

[3]Institute of Physics, Chinese Academy of Science, Beijing 100190, China

Ferromagnetism in perovskites $RTiO_3$ can be induced by a steric effect. How the subtle local structural change can induce 3D ferromagnetic coupling through Ti-O-Ti superexchange interactions remains controversial. The critical behavior study for the ferromagnetic phase has been made so far only on $YTiO_3$ since the magnetization measurements are plagued by the contribution from magnetic rare earth. Here we report critical exponents for most ferromagnetic members in the $RTiO_3$ family by measuring magnetocaloric effect and applying the corresponding scaling laws. Our results indicate that the ferromagnetic coupling in the $RTiO_3$ can be well-described by the 3D Heisenberg model.

PACS numbers: 75.40.Cx, 75.47.Lx, 75.30.Sg

For a second-order ferromagnetic phase transition, the critical behavior near T_c is characterized by a set of critical exponents[1] α, β, γ, and δassociated with, respectively, the specific heat C, the spontaneous magnetization $M_s(\equiv M_{H=0})$, the initial magnetic susceptibility $\chi_0(\equiv \partial M/\partial H|_{H=0})$, and the critical isothermal $M(H)_{T=Tc}$ through the following equations:

$$C(T) \sim |T-T_c|^{-\alpha}, \qquad (1)$$

$$M_s(T) \sim |T-T_c|^{\beta} \ (T < T_c), \qquad (2)$$

$$\chi_0(T) \sim |T-T_c|^{-\gamma} \ (T > T_c), \qquad (3)$$

$$M(H) \sim H^{1/\delta} \ (T = T_c). \qquad (4)$$

These critical exponents are not independent and the number of independent variables is reduced to two by the following relations:

$$\alpha + 2\beta + \gamma = 2, \qquad (5)$$

$$\delta = 1+\gamma/\beta. \qquad (6)$$

Precise determination of these critical exponents can provide valuable information about a magnetic phase transition, *e.g.* the range and the dimensionality of the magnetic exchange interactions[2]. As shown in Table I, distinct values of the critical exponents corresponding to different models have been derived theoretically[1]. The mean-field model with $\alpha = 0$, $\beta = 0.5$, and $\gamma = 1$ signals a long-range exchange interaction with negligible critical fluctuations near T_c. Such critical behaviors are usually observed in the very weak itinerant-electron ferromagnetic systems, *e.g.* $ZrZn_2$[3], which have been justified theoretically by Stoner and Wohlfarth. In contrast, the three-dimensional (3D) Heisenberg model involves isotropic nearest-neighbor exchange interactions between localized spins; significant critical fluctuations in the vicinity of T_c lead to $\beta < 0.5$ and $\gamma > 1$. Such a universality class has been found experimentally in a wide range of ferromagnetic systems, including metallic Ni[4], CrO_2[5], $La_{1-x}A_xMnO_3$[6], and insulating $YTiO_3$[7,8]. Although the 3D Ising model is applicable when the spin degree of freedom is restricted to one direction, an experimental realization of the 3D Ising ferromagnetism in real system is rare[9].

For a critical behavior analysis around a second-order ferromagnetic transition, the most straightforward and widely used approach is the Arrott-plot method[10] based on dc magnetization measurements. For this purpose, a series of isothermal magnetization M(H) curves around T_c is replotted in the form of M^2 versus H/M, *i.e.* the Arrott plot. A parallel linear Arrott plot signals the mean-field universality class with $\beta = 0.5$ and $\gamma = 1$. However, in most cases the Arrott plot does not

produce straight lines. In order to determine precisely the critical exponents, these isotherms in the Arrott plot are usually fitted with a polynomial function and then extrapolated to the H/M = 0 and M^2 = 0 axes to obtain the spontaneous magnetization M_s and the initial magnetic susceptibility χ_0, respectively. Then, a power law fitting to $M_s(T)$ and $\chi_0(T)$ according to Eqs. (2) and (3) yields the values of β and γ, respectively. By using these critical exponents as a starting point, a modified Arrott plot, $M^{1/\beta}$ versus $(H/M)^{1/\gamma}$, can be obtained and the above procedures can be applied again to get new values of β and γ. Such an iteration process can be applied until the critical exponents β and γ converge. Parallel straight isothermal lines should be restored in the modified Arrott plot with the correct critical exponents.

For most homogeneous ferromagnetic systems involving only one magnetization process, the above-mentioned Arrott-plot method is applicable. Otherwise, application of this method requires caution; interpretation of the obtained critical exponents must take into account the specific situation of the magnetic system. For example, in the $RTiO_3$ (R = Gd, …,Lu, and Y) perovskites, the critical behavior associated with the ferromagnetic ordering of the localized Ti^{3+} S = ½ spin can be well understood in terms of the 3D Heisenberg model as shown in $YTiO_3$. However, in these ferromagnetic $RTiO_3$ (R ≠ Y and Lu), the presence of large paramagnetic R^{3+} moments near T_c makes the Arrott-plot method invalid for the critical-behavior analysis. As shown in the present study on $RTiO_3$, the Arrott-plot approach even leads to an opposite conclusion. Interestingly, during the course of our study on the magnetocaloric effect (MCE) of these ferromagnetic $RTiO_3$[11], we found that the correct critical exponents can be deduced from the MCE scaling laws[12].

For a magnetic system with a second-order phase transition, Oesterreicher and Parker[14] have proposed a universal relation:

$$\left|\Delta S_M^{PK}\right| \propto H^n \quad \text{with } n = 2/3, \qquad (7)$$

where ΔS_M^{PK} is the peak value of the magnetic entropy change at different external magnetic fields H. Although subsequent experimental results in some soft magnetic amorphous alloys exhibit a deviation from n = 2/3[15], Franco *et al*.[12,16] recently confirmed the existence of the above universal relation and provided a new relation, *i.e.* the MCE scaling law:

$$n = 1 + (\beta - 1)/(\beta + \gamma), \qquad (8)$$

which is in better agreement with the experimental results. In addition, the relative cooling power (RCP)

obeys the scaling law:

$$RCP \propto H^{1+1/\delta}. \qquad (9)$$

According to Eqs. (6-9), we can deduce the critical exponents β and γ by determining the values of n and δ from the field dependences of ΔS_M^{PK} and RCP, respectively. Here we report critical exponents for most ferromagnetic members in the $RTiO_3$ family by measuring the magnetocaloric effect and applying the corresponding scaling laws. Our results indicate that the ferromagnetic coupling in the $RTiO_3$ can be well-described by the 3D Heisenberg model. The present study on $RTiO_3$ perovskite demonstrates that the MCE scaling laws can provide an alternative approach to investigate the critical behavior of a magnetic phase transition involving a strong paramagnetic background.

Single crystal $RTiO_3$ was grown by the floating-zone method as described elsewhere[7]. The phase purity and crystal quality were examined with powder X-ray diffraction and Laue back diffraction, respectively. DC magnetization and specific-heat measurements were performed with a Physical Property Measurement System (PPMS-9T) from Quantum Design.

Figure 1 shows the temperature dependence of magnetization M(T) for an $YbTiO_3$ single crystal measured upon warming up from 10 to 70 K under an external magnetic field H = 0.01 T after zero-field cooling (ZFC). The ferromagnetic ordering of the Ti^{3+} spins induces an abrupt increase in M(T) around T_C = 42.5 K, leading to a large magnetic entropy change. The field-cooled cooling (FCC) and field cooled warming (FCW) M(T) curves (inset of Fig. 1) do not show any thermal hysteresis around T_C, indicating a second-order magnetic phase transition. At temperatures slightly below T_c, the magnetization decreases sharply until ca. 30 K, where the M(T) curve exhibits a noticeable shoulder. In comparison with the typical ferromagnetic behavior observed in $YTiO_3$[7], these features should arise from the large Yb^{3+} moments and indicate an antiparallel alignment relative to the ferromagnetic Ti^{3+} spins. As shown below by the specific-heat data, the Yb^{3+} moments do not show a long-range ordering at least down to 20 K. The large paramagnetic contribution of the Yb^{3+} moments makes it invalid to evaluate the critical behavior near T_c with the conventional Arrott-plot method. Similar results are also found in the other $RTiO_3$ with magnetic R^{3+} (R=Dy, Ho, Er, Tm).

As shown in Fig. 2, the Arrott plots of the $RTiO_3$ single crystals produce nearly parallel straight lines both below and above T_C, which seem to suggest that the critical behavior of $RTiO_3$ fits to the mean-field universality class[13]. The critical exponents, β and γ, obtained with the conventional Arrott-plot procedure, are also close to those predicted by the mean-field model (see Table I). However,

it has been well-established in $YTiO_3$ that the critical behavior associated with the ferromagnetic ordering of the Ti^{3+} spins belong to the 3D Heisenberg universality class[7,8]. In addition, the nearest-neighbor exchange interactions between localized Ti^{3+} spins in these ferromagnetic $RTiO_3$ do not fit into the mean-field model. The large paramagnetic R^{3+} moments contribute to a linear-field dependence in the isothermal M(H) curves around T_c, which modifies significantly the magnetization process and then leads to a different model of magnetic interactions based on the conventional Arrott-plot method. In the following, we show that the correct critical exponents of $RTiO_3$ can be deduced from the magnetocaloric-effect (MCE) scaling laws.

We have shown recently that the magnetic transitions of the ferromagnetic $RTiO_3$ are accompanied by a large magnetocaloric effect[11]. Here, we applied the above-mentioned MCE scaling laws to evaluate the critical behavior of $RTiO_3$. In order to obtain the values of n and δ, we first calculated the magnetic entropy change versus temperature under different magnetic fields by using the Maxwell relation: $\Delta S_M(T,\Delta H)=\int_0^H\left(\frac{\partial M}{\partial T}\right)_H dH$. Then, the relative cooling power (RCP, evaluated by $RCP=\Delta S_M^{PK}\times\delta T_{FWHM}$[18]) can be deduced from the ΔS_M versus T curves. The calculated $\Delta S_M(T)$ under different magnetic fields for $RTiO_3$ are shown in Fig. 3(a)-(e), while the field dependences of ΔS_M^{PK} and RCP are plotted in Fig. 3(f)-(j). As shown by the solid lines in Fig. 3(f)-(j), least-square fittings to $\Delta S_M^{PK}(H)$ and RCP(H) with Eqs. (7) and (9) yields the values of n and δ, respectively. Finally, with the help of Eqs. (6) and (8), the critical exponents β and γ of $RTiO_3$ were determined, respectively. These values are in sharp contrast with those obtained from the Arrott-plot method shown above. As shown in Table I, the critical exponents β and γ of $RTiO_3$ are close to those predicted by the 3D Heisenberg model and are in excellent agreement with those of $YTiO_3$[7,8].

The reliability of our above critical-behavior analysis for $RTiO_3$ was further confirmed by the scaling plot of the magnetic entropy change ΔS_M,[16,17] which can be expressed as $\Delta S_M/a_M = H^n s(t/H^{1/\Delta})$, where $a_M = T_C^{-1}A^{\delta+1}B$ with A and B the critical amplitudes as in $M_S(T) = A(-t)^\beta$ and $H = BM^\delta$, respectively, $\Delta=\beta\delta$, and $s(x)$ is the scaling function. If the reduced temperature t was rescaled by a factor $H^{1/\Delta}$ and the magnetic entropy change ΔS_M by H^n, the experimental data should collapse onto the same curve. For instance, by using the values of β = 0.355, γ = 1.402 and δ = 4.95 obtained above, we have obtained the scaling plot of Fig. 4 for our $YbTiO_3$ single crystal. As can be seen, except for the low temperature region at $T < T_C$, all data points indeed fall onto the same curve. Therefore, the MCE

scaling method is an effective and reliable approach to investigate the critical behavior of $RTiO_3$ having a strong paramagnetic background near T_c.

To complete the critical-behavior analysis, we have further determined the critical exponent α from the specific-heat measurement. Fig. 5 shows the specific heat C(T) of $RTiO_3$ in the temperature range near T_c. In the critical region, C(T) data can be described by a more sophisticated function[19]:

$$C_p = B^{\pm} + C^{\pm}t + A^{\pm}\left|t\right|^{-\alpha}(1 + E^{\pm}\left|t\right|^{0.5}), \quad (10)$$

where $t = (T - T_C)/T_C$ is the reduced temperature, α is the critical exponent, and $A^{\pm}$, $B^{\pm}$, $C^{\pm}$ and $E^{\pm}$ are adjustable parameters. Superscripts + and – stand for $T > T_C$ and $T < T_C$, respectively. The linear term represents the background contribution to the specific heat whereas the last term is the anomalous contribution to the specific heat. The factor within parentheses is the correction to scaling that represents a singular contribution to the leading power as known from experiments and theory[20,21]. As shown by the continuous line in Fig. 5, the experimental data can be described excellently with Eq. (10). The obtained critical parameters, adjustable fitting parameters (such as A, B, C and E), the fitting ranges and the quality of the fittings (given by the root mean square value) were listed in the Table II. The fitting reduced temperature t ranges is about 10^{-1}~10^{-3} in the vicinity of the Curie temperature T_C while avoiding the rounding part[22]. The root mean square values R^2 is close to 1, indicating the validity of the fitting. The fitting ranges are in all cases limited by the rounding in the curves near the transition temperature; this rounding is inherent to the quality of the samples and the attribution to the measurement technique[22]. The obtained α (see Table I and Table II) for $RTiO_3$ single crystal is in excellent agreement with the prediction of the 3D Heisenberg model[13, 23], further supporting the above analysis with the MCE scaling laws. Critical exponents α, β, and γ of $RTiO_3$ obtained in this study satisfy Eq. (5), $\alpha + 2\beta + \gamma = 2$, which also indicates that the critical exponents obtained by the MCE scaling law method is valid.

Finally, let's briefly comment on the merit of t he MCE scaling laws, which can overcome the drawback of the conventional Arrott-plot method by avoiding the influence of the paramagnetic R^{3+} moments on the critical behavior of $RTiO_3$. In the critical region where the Ti^{3+} spins undergo a sharp ferromagnetic ordering, the R^{3+} moments remain paramagnetic and vary smoothly with temperature without singularity. Since the magnetic entropy change ΔS_M is proportional to the temperature derivative of the magnetization, dM/dT, the paramagnetic 'background' from the R^{3+} moments can be

eliminated. In other words, the magnetocaloric effect at the Curie temperature T_C mainly reflects the ferromagnetic ordering behavior of the Ti^{3+} spins. Therefore, the MCE scaling laws is valid to investigate the critical behavior of $RTiO_3$.

In summary, we have determined that the critical behavior in $RTiO_3$ single crystals belongs to the 3D Heisenberg universality class by using the MCE scaling laws, which also agrees with the specific-heat measurement. This approach not only eliminates the influence of other paramagnetic contributions in the critical region; it also avoids the drawback of the iteration procedure in the conventional Arrott-plot method. Therefore, the MCE scaling laws can be applied to complex magnetic systems involving different magnetization process in the critical region.

Acknowledgements

This work was supported by the National Natural Science Foundation of China (Grant No. 10804024) and the NSF MIRT (DMR-1122603) in USA.

*suiyu@hit.edu.cn

[1] H. E. Stanley, *Introduction to phase transition and critical phenomena* (Oxford University Press, New York, 1971).

[2] M. E. Fisher, S. K. Ma, and B. G. Nickel, Phys. Rev. Lett. **29**, 917 (1972).

[3] M. Seeger, H. Kronmüller, and H. J. Blythe, J. Magn. Magn. Mater. **139**, 312 (1995).

[4] M. Seeger, S. N. Kaul, H. Kronmüller, and R. Reisser, Phys. Rev. B 51, 12585 (1995).

[5] F. Y. Yang, C. L. Chien, X. W. Li, G. Xiao, and A. Gupta, Phys. Rev. B **63**, 092403 (2001).

[6] J. Yang, Y. P. Lee, and Y. Li, Phys. Rev. B **76**, 054442 (2007), and references herein.

[7] J.-G. Cheng, Y. Sui, J.-S. Zhou, J. B. Goodenough, and W. H. Su, Phys. Rev. Lett. **101**, 087205 (2008).

[8] W. Knafo, C. Meingast, A. V. Boris, P. Popovich, N. N. Kovaleva, P. Yordanov, A. Maljuk, R. K. Kremer, H. v. Löhneysen, and B. Keimer, Phys. Rev. B **79**, 054431 (2009).

[9] J.-G. Cheng, J.-S. Zhou, J. B. Goodenough, Y. T. Su, and Y. Sui, Phys. Rev. B **83**, 212403 (2011).

[10] A. Arrott and J. E. Noakes, Phys. Rev. Lett. **19**, 786 (1967).

[11] Y. T. Su, Y. Sui, J.-G. Cheng, X. J. Wang, Y. Wang, W. F. Liu, and X. Y. Liu. J. Appl. Phys. **110**,

083912 (2011).

[12] V. Franco, and A. Conde, Int. J. Refrig. **33**, 465 (2010).

[13] H. E. Stanley, Rev. Mod. Phys. **71**, S358 (1999).

[14] H. Oesterreicher and F. T. Parker, J. Appl. Phys. **55**, 4334 (1984).

[15] Q. Y. Dong, H. W. Zhang, J. R. Sun, B. G. Shen, and V. Franco, J. Appl. Phys. **103**, 116101 (2008).

[16] V. Franco, A. Conde, J. M. Romero-Enrique, and J. S. Blazquez, J. Phys.: Condens. Matter **20**, 285207 (2008).

[17] C. M. Bonilla, J. Herrero-Albillos, F. Bartolomé, L. M. García, M. Parra-Borderías, and V. Franco, Phys. Rev. B **81**, 224424 (2010).

[18] B. Li, J. Du, W. J. Ren, W. J. Hu, Q. Zhang, D. Li, and Z. D. Zhang, Appl. Phys. Lett. **92**, 242504 (2008).

[19] A. Salazar, M. Massot, A. Oleaga, A. Pawlak, and W. Schranz, Phys. Rev. B **75**, 224428 (2007).

[20] G. Ahlers, Rev. Mod. Phys. **52**, 489 (1980).

[21] A. Aharony and M. E. Fisher, Phys. Rev. B **27**, 4394 (1983).

[22] A. Oleaga, A. Salazar, D. Prabhakaran, J.-G. Cheng, and J.-S. Zhou, Phys. Rev. B **85**, 184425 (2012)

[23] V. Privman, P. C. Hohenberg, and A. Aharony, in *Phase Transitions and Critical Phenomena*, edited by C. Domb and J. L. Lebowitz (Academic, New York, 1991), Vol. 14.

Table Captions:

TABLE I. Critical exponents of $RTiO_3$ obtained from the conventional Arrott-plot method and the MCE scaling law method and theoretical values of three models.

TABLE II. Critical parameters, adjustable fitting parameters, fitting ranges and quality of the fittings of the specific heat for $RTiO_3$. *R* is the deviation coefficient.

Figure Captions:

FIG. 1. Temperature dependence of the magnetization measured at H = 0.01 T after zero-field cooling for a $YbTiO_3$ single crystal. Inset: Magnetization vs. temperature curves in the field-cooled cooling and warming cycles under a magnetic field of 1 T.

FIG. 2. (a)-(e) Arrott plots M^2 versus H/M for $RTiO_3$, respectively. (f)-(j) Critical exponents, β and γ, and critical temperatures, T_C^- and T_C^+, determined from an iteration process started from the Arrott plot for $RTiO_3$, respectively.

FIG. 3. (Color online) (a)-(e) Temperature dependence of the magnetic entropy changes ΔS_M under various external magnetic fields. (f)-(j) Field dependence of the maximal ΔS_M and the RCP and their fitting curves using the MCE scaling laws.

FIG. 4. (Color online) Scaling plot for $YbTiO_3$ below and above T_C based on the critical exponents β = 0.355, γ = 1.402 and δ = 4.95 [where $n = 1 + (\beta - 1)/(\beta + \gamma)$ and $\Delta = \beta\delta$].

FIG. 5. Experimental (squares) and fitted curves (continuous lines) of the specific heat as a function of the reduced temperature for the $RTiO_3$ in the vicinity of T_c.

TABLE I.

		α	β	γ	δ	Ref.
Mean-field model		0	0.5	1.0	3.0	13
3D Ising model		0.11	0.325	1.241	4.82	13
3D Heisenberg model		-0.11	0.365	1.386	4.80	13
Arrott plot method	$DyTiO_3$	….	0.328(3)	1.119(2)	….	This work
	$HoTiO_3$	….	0.481(4)	1.032(2)	….	This work
	$ErTiO_3$	….	0.462(5)	0.919(2)	….	This work
	$TmTiO_3$	….	0.460(7)	1.078(2)	….	This work
	$YbTiO_3$	….	0.432(8)	1.062(3)	….	This work
	$YTiO_3$	-0.11 [a]	0.328(4)	1.441(5)	4.85(2)	7
MCE scaling law method	$DyTiO_3$	-0.110(3) [a]	0.352(2)	1.355(3)	4.85(2)	This work
	$HoTiO_3$	-0.110(5) [a]	0.397(5)	1.476(4)	4.72(6)	This work
	$ErTiO_3$	-0.106(3) [a]	0.413(5)	1.611(6)	4.90(5)	This work
	$TmTiO_3$	-0.110(1) [a]	0.401(4)	1.427(3)	4.56(5)	This work
	$YbTiO_3$	-0.109(3) [a]	0.355(4)	1.402(3)	4.95(3)	This work

[a] The critical exponent α calculated from the specific heat data.

TABLE II.

		α	T_C (K)	A (J mol^{-1} K^{-1})	B (J mol^{-1} K^{-1})	C (J mol^{-1} K^{-1})	E	t_{min}-t_{max}	R^2
$DyTiO_3$	$T<T_C$	-0.110(3)	64.7 (9)	-13.5(6)	74.6(4)	9.04(9)	6.35(7)	$2.3\times10^{-1} - 7.7\times10^{-3}$	0.9999
	$T>T_C$	-0.110(1)	65.1 (5)	-30.0(3)	55.4(6)	28.04(4)	-0.50(2)	$7.7\times10^{-3} - 2.3\times10^{-1}$	0.9989
$HoTiO_3$	$T<T_C$	-0.110(5)	50.7 (4)	-10.0(2)	48.0(9)	-97.75(3)	-2.22(9)	$2.1\times10^{-1} - 9.8\times10^{-3}$	0.9993
	$T>T_C$	-0.109(2)	50.8 (6)	-200.6(3)	144.1(4)	-217.0(2)	-1.341(3)	$3.9\times10^{-3} - 1.8\times10^{-1}$	0.9951
$ErTiO_3$	$T<T_C$	-0.106(3)	41.7(9)	-5.0(2)	20.4(5)	-21.3(3)	0.044(1)	$1.6\times10^{-1} - 7.2\times10^{-3}$	0.9998
	$T>T_C$	-0.108(1)	42.0(1)	-22.7(3)	25.6(4)	-5.90(4)	-0.88(7)	$9.6\times10^{-3} - 2.0\times10^{-1}$	0.9938
$TmTiO_3$	$T<T_C$	-0.110(1)	65.2(2)	-3.11(2)	54.7(4)	-49.7(3)	7.65(1)	$2.1\times10^{-1} - 7.7\times10^{-3}$	0.9998
	$T>T_C$	-0.110(1)	65.2(1)	-326.7(3)	226(4)	-242.3(2)	-1.09(3)	$7.7\times10^{-3} - 2.3\times10^{-1}$	0.9943
$YbTiO_3$	$T<T_C$	-0.109(3)	42.2(2)	-0.738(8)	32.23(2)	-4.78(3)	50.4(3)	$1.7\times10^{-1} - 4.8\times10^{-3}$	0.9998
	$T>T_C$	-0.110(3)	42.0(5)	-200(2)	135.3(1)	-168.8(2)	-1.18(8)	$7.1\times10^{-3} - 1.9\times10^{-1}$	0.9937

Figures:

FIG. 1.

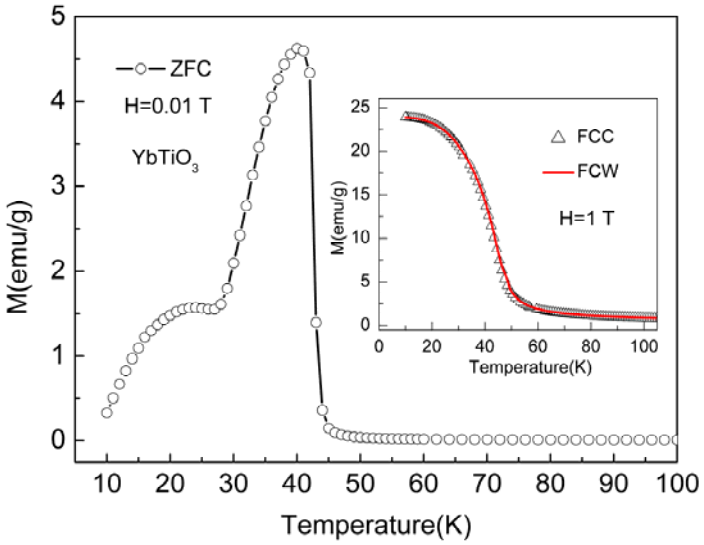

FIG. 2.

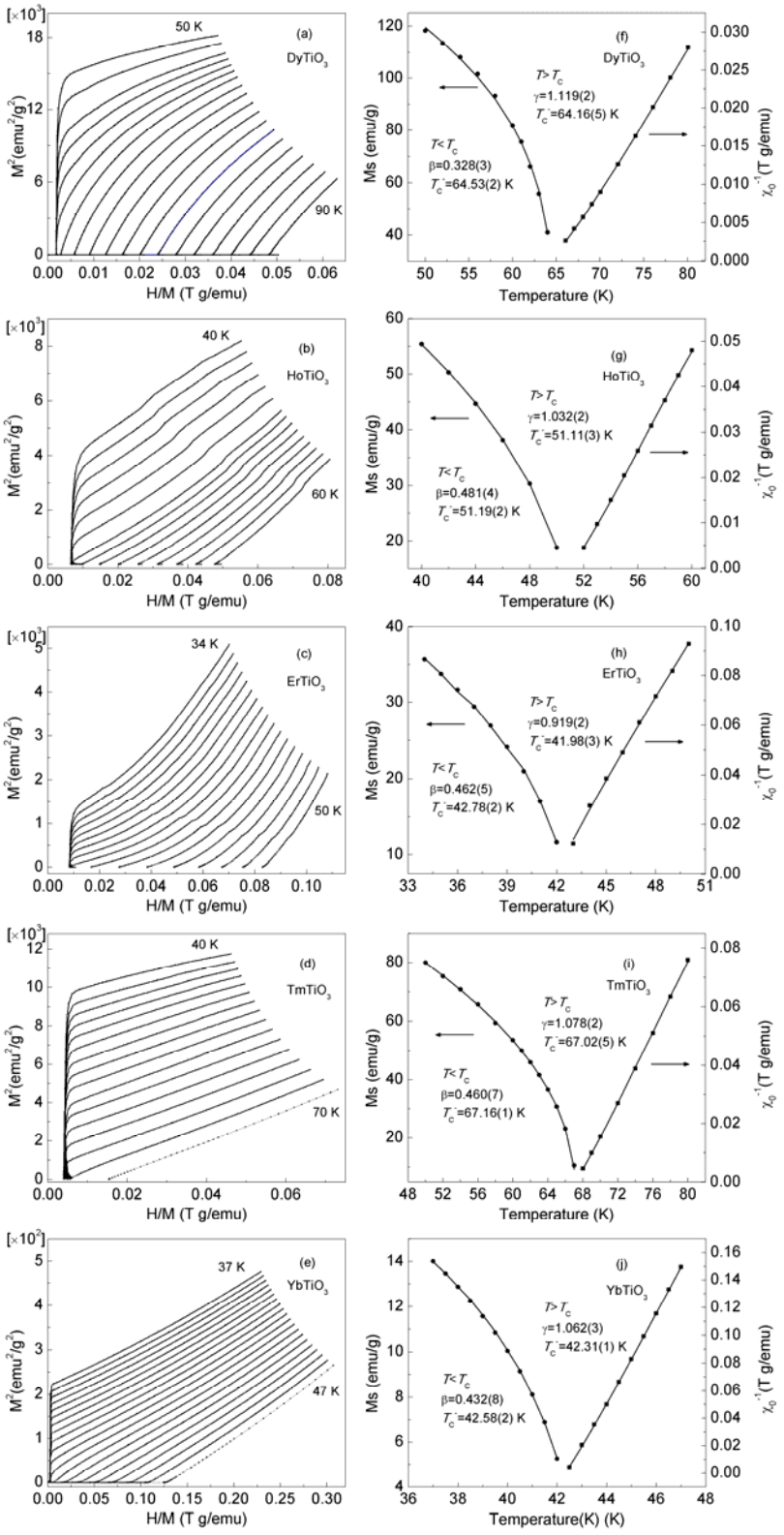
(a)
DyTiO3
50 K
90 K
M2(emu2/g2)
H/M (T g/emu)
(f)
DyTiO3
T> Tc
γ=1.119(2)
Tc=64.16(5) K
T< Tc
β=0.328(3)
Tc=64.53(2) K
Ms (emu/g)
χ0-1(T g/emu)
Temperature (K)
(b)
HoTiO3
40 K
60 K
(g)
HoTiO3
T> Tc
γ=1.032(2)
Tc=51.11(3) K
T< Tc
β=0.481(4)
Tc=51.19(2) K
(c)
ErTiO3
34 K
50 K
(h)
ErTiO3
T> Tc
γ=0.919(2)
Tc=41.98(3) K
T< Tc
β=0.462(5)
Tc=42.78(2) K
(d)
TmTiO3
40 K
70 K
(i)
TmTiO3
T> Tc
γ=1.078(2)
Tc=67.02(5) K
T< Tc
β=0.460(7)
Tc=67.16(1) K
(e)
YbTiO3
37 K
47 K
(j)
YbTiO3
T> Tc
γ=1.062(3)
Tc=42.31(1) K
T< Tc
β=0.432(8)
Tc=42.58(2) K
Temperature(K) (K)

FIG. 3.

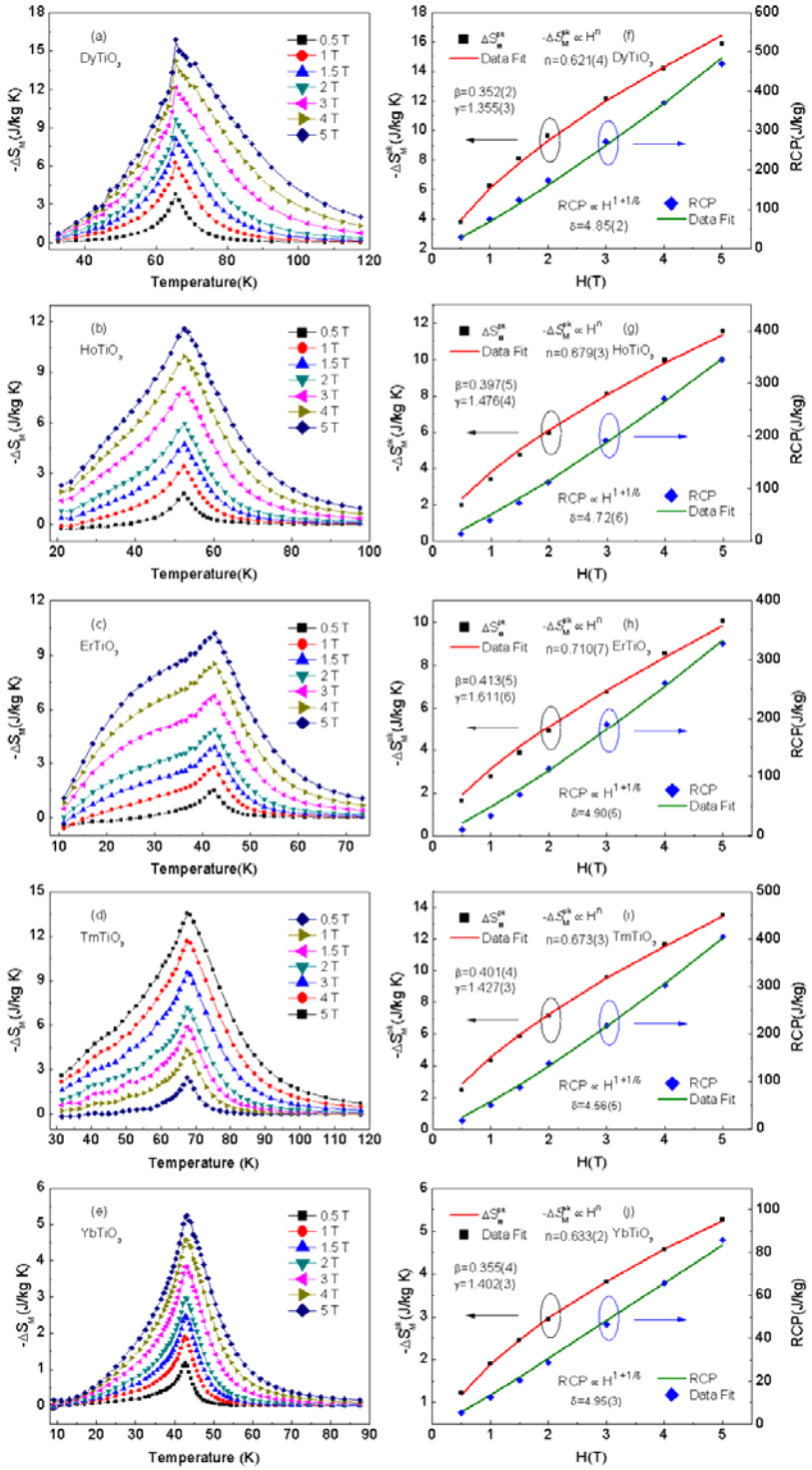
(a)
DyTiO3
0.5 T
1 T
1.5 T
2 T
3 T
4 T
5 T
-ΔSM (J/kg K)
Temperature(K)
(f)
DyTiO3
Data Fit
n=0.621(4)
β=0.352(2)
γ=1.355(3)
δ=4.85(2)
RCP
H(T)
RCP(J/kg)
(b)
HoTiO3
n=0.679(3)
β=0.397(5)
γ=1.476(4)
δ=4.72(6)
(g)
(c)
ErTiO3
n=0.710(7)
β=0.413(5)
γ=1.611(6)
δ=4.90(5)
(h)
(d)
TmTiO3
n=0.673(3)
β=0.401(4)
γ=1.427(3)
δ=4.56(5)
(i)
(e)
YbTiO3
n=0.633(2)
β=0.355(4)
γ=1.402(3)
δ=4.95(3)
(j)

FIG. 4.

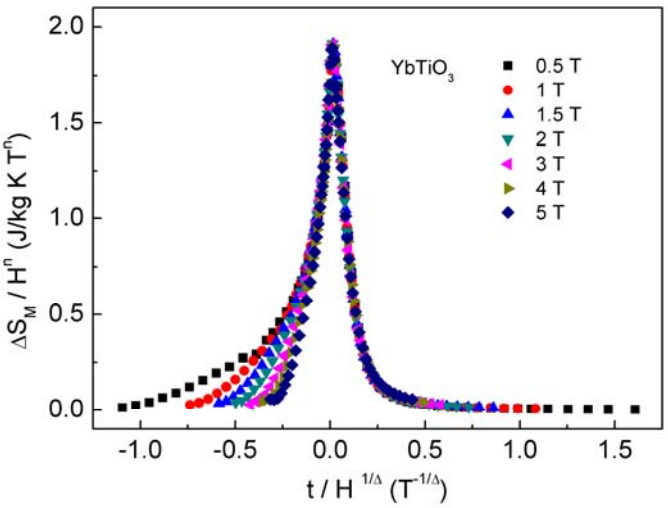
YbTiO3
0.5 T
1 T
1.5 T
2 T
3 T
4 T
5 T
ΔSM / Hn (J/kg K Tn)
t / H 1/Δ (T-1/Δ)
2.0
1.5
1.0
0.5
0.0
-1.0
-0.5
0.0
0.5
1.0
1.5

FIG. 5.

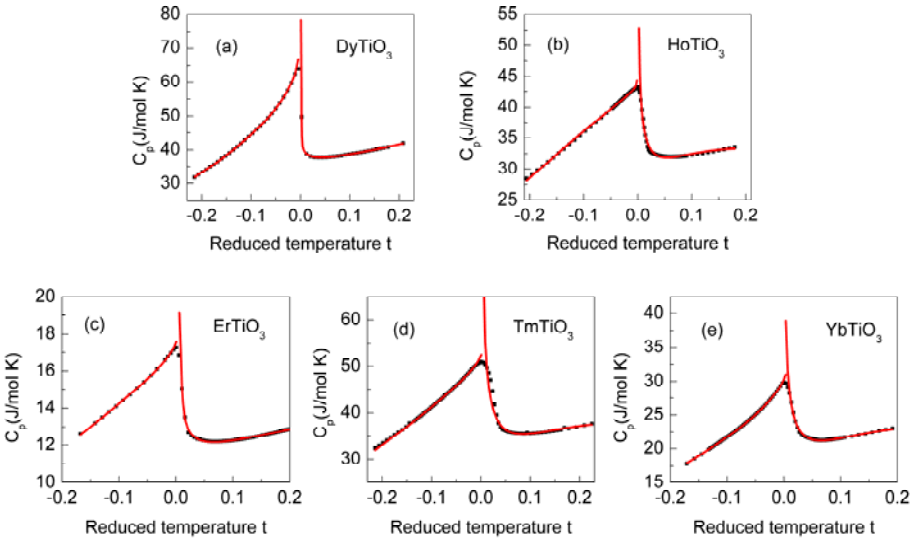
(a)
DyTiO3
(b)
HoTiO3
(c)
ErTiO3
(d)
TmTiO3
(e)
YbTiO3
Cp (J/mol K)
Reduced temperature t